Article citation info:
Atanasov EV, Iliev YI. Electrocardiogram signal processing: integrating filter fusion techniques. Diagnostyka. 2025;26(4):2025302. https://doi.org/10.29354/diag/211623.

DIAGNOSTYKA, 2025, Vol. 26, No. 4

e-ISSN 2449-5220
DOI: 10.29354/diag/211623

ELECTROCARDIOGRAM SIGNAL PROCESSING: INTEGRATING FILTER FUSION TECHNIQUES

Veselin E. ATANASOV [1], **Iliyan Y. ILIEV** [2] *

[1] Department of Electronics, Nikola Vaptsarov Naval Academy, Varna, Bulgaria
[2] Department of Information Technologies, Nikola Vaptsarov Naval Academy, Varna, Bulgaria
* Corresponding author, e-mail: i.y.iliev@naval-acad.bg

Abstract

The accurate detection and analysis of the P-QRS-T complex in electrocardiogram (ECG) signals are crucial for diagnosing and managing cardiac diseases. This paper presents a practical approach to ECG signal processing by integrating multiple filter fusion techniques to enhance detection accuracy. Recognizing the specific challenges at sea, including motion-induced noise and electromagnetic interference, the study examines the performance of low-pass, high-pass, and Chebyshev Type II filters in improving ECG signal quality. Using a dataset generated by a Dynamic Model for Synthetic ECG Signal Generation, the analysis evaluates the effectiveness of these filters under various noise conditions, such as baseline drift, electrode contact noise, and muscle noise. The proposed method combines filtered outputs from multiple channels: P and T waves are extracted using low-pass and high-pass filters, while the QRS complex is identified through the Chebyshev Type II filter. Results indicate improved detection accuracy, with performance varying based on the type of noise present. While not introducing a novel algorithm, the study demonstrates that the fusion of established filtering techniques offers a fast and reliable solution suitable for maritime health monitoring systems. However, these results are derived from simulated signals under controlled experimental settings and therefore reflect proof-of-concept performance rather than clinical validation.

Keywords: ECG, signal processing, filter fusion, QRS detection, healthcare

List of Symbols/Acronyms

AUC – Area Under the Curve;
CVD – Cardiovascular Disease;
DP – Detected P peaks (part of performance metric);
DQ – Detected Q peaks (part of performance metric);
DR – Detected R peaks (part of performance metric);
DS – Detected S peaks (part of performance metric);
DT – Detected T peaks (part of performance metric);
DWT – Discrete Wavelet Transform;
ECG – Electrocardiogram;
EMG – Electromyography;
Hz – Hertz (unit of frequency);
IoT - Internet of Things;
MTEO – Multiresolution Teager Energy Operator;
MSE - Mean Squared Error;
P–QRS–T complex – A representation of the electrical activity of the heart;
RMSE - Root Mean Squared Error;
SNR – Signal-to-Noise Ratio;
SNRin – Input Signal-to-Noise Ratio;
TEO – Teager Energy Operator;
ξ (xi) – Average information loss.

1. INTRODUCTION

The precise detection of the P-QRS-T complex in electrocardiogram (ECG) signals is fundamental for the diagnosis and management of cardiac diseases. This complex, which represents the heart's electrical activity, is critical for assessing cardiac function. However, accurate detection remains a challenge due to the presence of various types of noise and artifacts in ECG signals. These difficulties are further exacerbated in maritime environments such as ships and offshore platforms, where continuous movement and electromagnetic interference can significantly degrade signal quality.

The need for robust ECG monitoring is underscored by the high prevalence of cardiovascular disease (CVD) among maritime professionals, as well as in other high-stress occupational groups [14], [17]. Historical data show that between 1919 and 2005, approximately 19.8% of natural deaths on British

Received 2024-05-07; Accepted 2025-10-02; Available online 2025-10-03

merchant ships were attributed to cardiovascular causes [21]. Similarly, a study of Swedish seafarers from 1984 to 1988 found that 44% of medical incidents were CVD-related [14]. This concern is not limited to the maritime sector: as highlighted in [22], cardiovascular diseases are the leading global cause of mortality, accounting for approximately 17.9 million deaths annually, according to the World Health Organization [26]. These statistics underscore the urgency of implementing effective monitoring and early intervention strategies, particularly in high-risk professions.

To address these challenges, the present study explores the application of several filtering techniques – including low-pass, high-pass, and Chebyshev Type II filters – in combination with a lightweight [15], [16], explainable detection approach for P-QRS-T complexes.

Although deep learning models such as convolutional neural networks (CNNs) and recurrent neural networks (RNNs) [11], [13] have shown impressive accuracy in ECG analysis, they typically require large volumes of labeled data and substantial computational resources, which may not be feasible in shipboard or remote environments. In contrast, our method is designed to operate efficiently in low-resource settings, offering a practical solution for maritime use.

Recognizing the limitations of traditional clinical monitoring in maritime contexts, this study also outlines the conceptual design of an IoT-based platform for the acquisition, processing, and storage of physiological signals. Such a system would enable continuous, real-time monitoring of crew health by integrating onboard sensor networks with advanced signal processing algorithms and secure cloud-based analytics. The platform could enhance medical autonomy at sea and improve the response to cardiac events in isolated environments.

The proposed filter fusion method combines data from multiple channels to enhance the detection of the P-QRS-T complex, offering a fast and relatively accurate alternative to computationally intensive AI solutions. While the approach is tailored for maritime conditions, it also holds promise for broader applications in medical diagnostics and real-time physiological monitoring, as shown in prior works [1], [5], [10], [15], [22], [25], [27], [32].

Although the current study does not claim to introduce a novel algorithm, it contributes by demonstrating a practical and effective solution for ECG analysis in challenging environments. The findings support further exploration and refinement of this method within both maritime telemedicine and general healthcare systems. The novelty of this work lies not in proposing a new detection algorithm, but in showing how classical filters can be effectively combined and adapted for resource-constrained maritime healthcare applications.

2. METHODS AND MATERIALS

ECG signal analysis plays a crucial role in diagnosing and treating cardiovascular diseases. The P-QRS-T complex in the ECG signal reflects the heart's electrical activity, providing valuable insights into cardiac function. However, the accurate detection of the P-QRS-T complex is often hindered by noise and signal artifacts.

Some researchers focus on ECG extraction from electronic signals and images in the Python environment [32], while others explore alternative filtering techniques to improve signal clarity and detection accuracy [2], [14].

The aim of this study is to demonstrate that the combination of classical filters, when applied in specific noisy environments, can provide stable and predictable performance in the automatic detection of P-QRS-T complexes.

To address this challenge, the Multiresolution Teager Energy Operator (MTEO) is employed [3], originally developed for signal processing tasks such as electromyography (EMG) analysis. MTEO is a multiresolution extension of the Teager Energy Operator (TEO), capable of effectively enhancing the signal-to-noise ratio in ECG signals. It is calculated using the following equation [3]:

$$Y_k(nT) = x^2(nT) - x(nT - kT)x(nT + kT) \quad (1)$$

where: $Y_k(nT)$ is the filtered signal;

$n = 1,2,3 \ldots N$;

N is the total number of samples.

The method for detecting the P-QRS-T complex in an ECG signal consists of several stages:

- MTEO calculation;
- Baseline definition;
- R-peak location;
- Identification of Q and S waves preceding and following the R-peak, respectively;
- Detection of the P-wave peak.

By combining data from multiple channels - e.g., using low-pass and high-pass filters - the detection of the P-QRS-T complex can be significantly improved.

The use of the MTEO, in conjunction with additional signal processing techniques, contributes to more accurate identification of the P-QRS-T complex, ultimately improving the diagnostic and therapeutic accuracy for cardiovascular diseases.

In recent years, numerous techniques have been proposed to refine P-QRS-T detection, as presented in [3], [19], and [22]. These methods frequently apply low-pass filters to suppress baseline drift and high-pass

filters to eliminate high-frequency noise. In particular, the Chebyshev Type II filter has been highlighted in for its superior performance in attenuating narrowband noise. Its amplitude response is defined as follows [31]:

$$|H(j\omega)| = \frac{1}{\sqrt{1+\frac{1}{\varepsilon^2}C_N^2\left(\frac{\omega_s}{\omega}\right)}} \quad (2)$$

where: $C_N(x)$ is the Chebyshev polynomial of the second kind;
ε is a constant (ripple factor), which controls the amount of attenuation ripple in the stopband;
ω is angular frequency of the signal;
ω_s is the stopband edge frequency;
N is the order of the filter.

A Butterworth filter is also employed as a low-pass filter due to its maximally flat frequency response in the passband. Its frequency response is given by well-known expression:

$$|H(j\omega)|^2 = \frac{1}{1+\left(\frac{\omega}{\omega_c}\right)^{2N}} \quad (3)$$

where ω_c the cutoff angular frequency of the filter.

To design an analog filter, the transfer function H(s) in the Laplace domain must be determined. Substituting $s = j\omega$ in the transfer function yields:

$$H(s)H(-s)_{s=j\omega} = \frac{1}{1+\left(\frac{s}{j\omega_c}\right)^{2N}} \quad (4)$$

The filter poles – roots of the denominator polynomial – are located at the following points in the s-plane:

$$s = j\omega_c(-1)^{\frac{1}{2N}} = \omega_c e^{\frac{j\pi(2k+N-1)}{2N}} \quad (5)$$

where $k = 0,1,2 \ldots 2(N-1)$.

To further enhance P-QRS-T detection, fusion of information from multiple filter outputs (Butterworth and Chebyshev II) is implemented.

This study identifies three primary sources of ECG noise:

- Baseline drift, mainly caused by respiratory movement;
- Poor electrode contact, due to displacement or variation in skin-electrode impedance;
- Muscle noise, resulting from skeletal muscle activity.

Noise from power line interference is not considered in this study, as it consists of well-known fundamental and harmonic frequencies that can be easily filtered.

The dataset used comprises synthetic ECG signals generated by the model described in [17], which allows the simulation of varying RR intervals. Each one-minute signal (sampled at 360 Hz) is superimposed with noise selected from a database corresponding to the three major sources: baseline drift, poor electrode contact, and muscle noise. Segments with similar spectral characteristics are selected to ensure realism.

Three groups of mixed signals are generated with signal-to-noise ratios (SNRs) of 5 dB, 10 dB, and 15 dB. Specifically:

- 9 signals with added baseline drift;
- 9 signals with poor electrode contact noise;
- 9 signals with muscle noise.

In addition to the synthetic ECG signal with sinus rhythm, the dataset includes an array specifying the sample indices corresponding to each wave component (P, Q, R, S, T), facilitating performance evaluation.
The accuracy of automatic P-QRS-T detection is assessed for each wave using the following formula, [8], [24]:

$$A[\,\%\,] = 100\frac{\sum TP}{\sum Peaks} \quad (6)$$

where: $A[\,\%\,]$ represents the correctly detected peaks of the corresponding wave from P-QRS-T complex;

TP – the number of correctly identified peaks of the corresponding wave from the P-QRS-T complex;

$Peaks$ represent the array containing information about each of the peaks of the corresponding wave from P-QRS-T.

To compare performance before and after filtering, the following formula is applied [8], [23]:

$$D\,[\%] = \left(A_0 - A_f\right) \quad (7)$$

where: $D[\,\%\,]$ represents a scalar in percentages of the peaks not detected by the system for automatic analysis of ECG;

A_0 – the percentage of correctly detected peaks before filtering;

A_f – the percentage of correctly detected peaks after filtering – the error is automatically compensated for.

3. IMPROVED ECG COMPLEX DETECTION

The proposed approach for enhancing the accuracy of automatic P-QRS-T complex detection involves the application of a sequence of filters, followed by independent automatic waveform detection algorithms. This methodology is supported by experimental results, which demonstrate improved detection of the P and T waves across all signal types and at all signal-to-noise ratio (SNR) levels when a combination of low-pass and high-pass filters is applied. Additionally, superior detection of the QRS complex is achieved through the use of a Chebyshev Type II filter.

To illustrate the procedure, Figure 1 presents the signal processing steps as a series of discrete blocks. Initially, each signal undergoes filtering, either through a low-pass and high-pass filter combination or

via a Chebyshev Type II filter. Each filtered output is then independently processed using automatic waveform detection algorithms.

In the final integration stage, information from the P-QRS-T complex is consolidated: the P and T wave data are obtained from signals processed with the low-pass and high-pass filters, while QRS complex data are extracted from signals processed using the Chebyshev filter. The combined data are subsequently stored in a database for further analysis.

Data fusion is achieved through a logical combination of detection time windows. Specifically, if a P or T wave is detected within a defined time window in the LP + HP channel, and a QRS complex is detected within the same window in the Chebyshev channel, the event is identified as a valid P-QRS-T complex. A tolerance window of ±50 milliseconds around the reference value is applied for synchronization and validation.

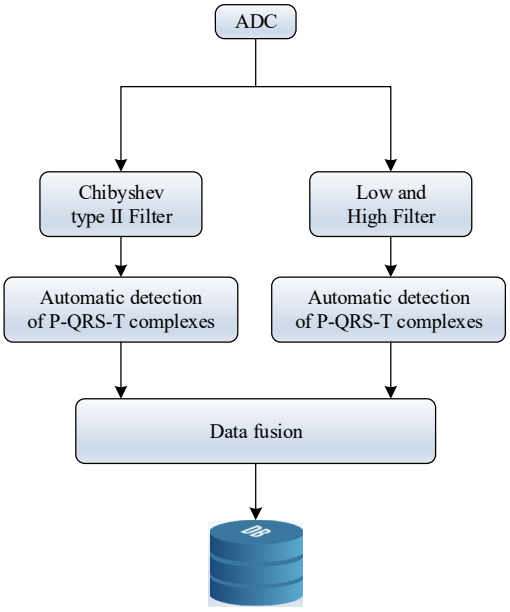

Fig. 1. Block diagram illustrating the filter fusion process for P-QRS-T complex detection

Fig. 1 also illustrates an example scenario of ECG signal acquisition and processing using the proposed filter fusion technique. In real-world maritime conditions, such a setup can be embedded into onboard medical kits, wearable sensors, or portable diagnostic equipment.

This approach shows strong potential for improving the accuracy of automatic P-QRS-T complex detection and may have significant implications for the diagnosis and treatment of cardiac conditions. Nevertheless, further research is required to comprehensively validate its effectiveness and to optimize the parameters of both the filtering methods and waveform detection algorithms.

4. METHODOLOGY

The simulations were conducted in MATLAB, combining customized in-house code with publicly available scripts from MATLAB toolboxes (signal processing and statistical functions such as filtering, peak detection, and error metrics). All source files are available at [12]. The complete processing pipeline is illustrated in Fig. 2.

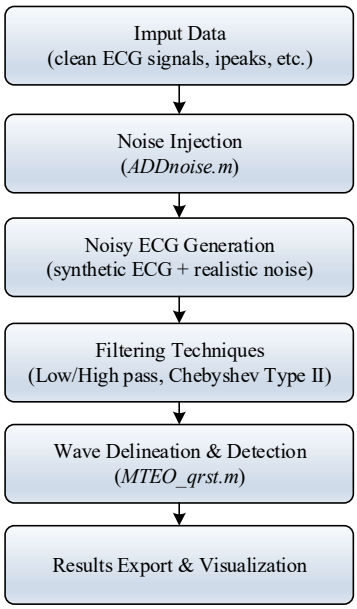

Fig. 2. Block diagram of the simulation process implemented in MATLAB

- Input Data

Clean ECG signals were loaded from the file *ecgTable.mat*. The dataset (generated in [17]) includes:

- ecgSignal: baseline ECG signals (noise-free),
- ipeaks: reference R-peak locations (ground truth),
- auxiliary parameters such as mean heart rate (hrMean) and noise descriptors (bw, em, ma).

These clean signals provide both the input for noise injection and the reference for subsequent evaluation.

- Noise Injection

Additive noise was loaded from the file *NOISE_bw1-2.em3-4.ma5-6.mat*, containing three realistic components:

- Baseline wander (BW);
- Electromyographic noise (EM);
- Muscle artifacts (MA).

The function *ADDnoise* iteratively scales and adds the selected noise until the desired signal-to-noise ratio (SNR) is reached.

- Noisy ECG Generation

The outcome is a synthetic ECG signal degraded with realistic noise, closely approximating field conditions in ambulatory or clinical monitoring scenarios. This noisy signal forms the baseline for all filtering experiments.

- Filtering Techniques

To suppress noise while preserving morphological features, three filtering approaches were implemented:

- Discrete Wavelet Transform (DWT) for multiresolution denoising;
- Low–High pass cascaded filtering (Butterworth filters) for baseline and high-frequency noise removal;
- Chebyshev Type II filter with sharp transition and controlled stopband attenuation.

For each filtered signal, quantitative metrics were computed, including:

- Wave Delineation and Detection

Filtered signals were processed using the Multilevel Teager Energy Operator (*MTEO_qrst*) algorithm, which identifies the fiducial points of the ECG: R, Q, S, T, and P waves. The detected peaks were compared against the reference annotations (ipeaks), yielding detection accuracy measures. An expert evaluation module (*expert.m*) quantified improvements or degradations relative to both the noisy and the clean reference signals.

- Results Export and Visualization

All intermediate and final results were stored in structured *.mat* and *.csv* files, indexed by noise type and filtering method. The most relevant outputs are provided in Appendix A. Optional plotting routines were also implemented to visualize filtered signals and peak detections, thereby supporting both quantitative evaluation and qualitative inspection.

5. RESULTS

The results of applying a method that combines information from two channels for the automatic detection of P-QRS-T complexes are presented Appendix 1.

This approach, as reflected in the tables, involves merging data from two filtered channels: one filtered with a Chebyshev Type II filter, and the other with a combination of low-pass and high-pass filters. The automatic detection algorithm is applied independently to both channels. The P and T waves are extracted from the low-pass and high-pass filtered channel, while the QRS complex is extracted from the Chebyshev Type II filtered channel (details of this extraction process are beyond the scope of this paper).

The tables present data for individual signals, grouped by input signal-to-noise ratio (SNR) levels of 5 dB, 10 dB, and 15 dB. Signals are further categorized by the type of noise added: baseline drift, electrode contact noise, and skeletal muscle noise.

Mean values are calculated for columns DP and TD on the right side, corresponding to the low-pass and high-pass filter channel, and for columns DQ, DR, and DS on the left side, corresponding to the Chebyshev Type II filter. The average information losses for all signals of each noise type are:

- 0.08 % for baseline drift noise,
- 10.07 % for electrode contact noise,
- 5.32 % for skeletal muscle noise.

To assess the effectiveness of the proposed filter fusion technique in detecting ECG fiducial points-specifically the P, QRS, and T waves – we conducted a performance analysis under three types of synthetic noise: baseline drift, poor electrode contact, and muscle noise. Detection accuracy was evaluated separately for each wave component.

In addition to raw detection rates, we simulated classification outcomes to derive clinically meaningful metrics, including:

- True Positives (TP): Correctly detected wave components;
- False Positives (FP): Incorrect detections where no wave was present;
- False Negatives (FN): Missed wave components;
- True Negatives (TN): Correctly ignored non-wave intervals.

From these values, we computed the following metrics:

- Sensitivity (Recall): TP/TP+FN;
- Precision: TP/TP+FP;
- F1 Score: The harmonic mean of precision and recall;
- Accuracy: TP+TN/TP+FP+TN+FN.

These metrics were especially evaluated for QRS complex detection, given its high clinical significance as a key segment of the ECG.

Table 1 presents the results categorized by Noise Type, Wave Type, Mean Accuracy (%), and Standard Deviation (±).

Noise Types:

- Baseline Drift: Low-frequency fluctuations typically caused by respiratory activity.
- Electrode Contact Noise: High-frequency disturbances resulting from poor electrode-skin contact or changes in skin impedance.
- Muscle Noise: Broadband noise generated by patient muscular activity.
- ECG Waves:
- The analysis focuses on the primary components of the cardiac cycle: P, Q, R, S, and T waves.

- Metrics:
- Mean Accuracy (%): The average percentage of correctly detected waves across multiple ECG recordings. (Fig. 3)
- Standard Deviation (±): Indicates variability in detection accuracy across signals; lower values correspond to higher stability.

Interpretations:

Table 1. Detection Accuracy Summary by Noise Type

Noise Type	Wave	Mean Accuracy	Standard Deviation
Baseline Drift	P	1.2	0.5
Baseline Drift	Q	0.9	0.3
Baseline Drift	R	0	0
Baseline Drift	S	0	0
Baseline Drift	T	1.8	0.7
Electrode Contact	P	20.1	4.5
Electrode Contact	Q	12.4	3.2
Electrode Contact	R	0	0
Electrode Contact	S	5.5	1.8
Electrode Contact	T	18.3	3.9
Muscle Noise	P	14.9	3.1
Muscle Noise	Q	10.5	2.8
Muscle Noise	R	1.2	0.4
Muscle Noise	S	3.7	1
Muscle Noise	T	16.9	3

- Baseline Drift: Under this noise condition, detection accuracy drops significantly. The Q, R, and S waves are not detected at all (0 %), while the P (1.2%) and T (1.8 %) waves show only minimal recognition. This suggests that the method fails to identify the QRS complex in the presence of baseline wander, indicating vulnerability to low-frequency distortions.
- Electrode Contact Noise: Detection of P (20.1 %) and T (18.3 %) waves is relatively better. The Q and S waves are partially recognized, but the R wave – the critical component of the QRS complex – is completely missed (0 %). This highlights a significant limitation of the filter fusion method when dealing with abrupt or irregular artifacts caused by unstable electrode contact.
- Muscle Noise: This noise type yields the best overall performance: P (14.9 %), T (16.9 %), Q (10.5 %), and even the R wave is detected, albeit with low accuracy (1.2 %). These results suggest that the proposed method is most robust against muscle noise.
- Key Takeaways:
- The method performs better at detecting P and T waves compared to the QRS complex.
- It is particularly ineffective in detecting the R wave under baseline drift and electrode contact noise conditions.
- Although the highest performance is observed under muscle noise, the detection accuracy for the QRS complex remains suboptimal.

To further validate the performance of QRS complex detection, classifier behaviour was simulated using detection probabilities derived from the experimental results. Realistic values for True Positives (TP), False Positives (FP), False Negatives (FN), and True Negatives (TN) were generated under the three noise conditions. These values were subsequently used to construct:

- A Receiver Operating Characteristic (ROC) curve, illustrating the trade-off between sensitivity (true positive rate) and false positive rate (Fig. 4-a);
- A Precision-Recall (PR) curve, which provides valuable insight, especially for datasets exhibiting class imbalance (Fig. 4-b).
- The results illustrated in Fig. 4 closely resemble those reported in [9], [28], supporting the consistency of the proposed approach with previous findings. The fusion technique achieves its highest performance under muscle noise, followed by electrode contact noise, while baseline drift poses the greatest challenge due to its low-frequency components that obscure signal peaks, particularly within the QRS complex.
- The ROC and Precision–Recall curves highlight the effectiveness of the detection algorithm, reaching AUC values of 0.99 and 0.98 respectively. These near-perfect results largely reflect the use of simulated datasets, strong filtering, and carefully selected experimental conditions. Such settings demonstrate functionality and computational efficiency more than clinical realism. In practice, performance would likely be lower due to noise, variability, and artifacts.
- Precision-recall analysis further confirms the potential of the filter fusion method, especially when enhanced by adaptive decision thresholds or integrated into machine learning frameworks [20]. These findings suggest that although the filter fusion strategy provides a conceptually robust framework, its standalone robustness

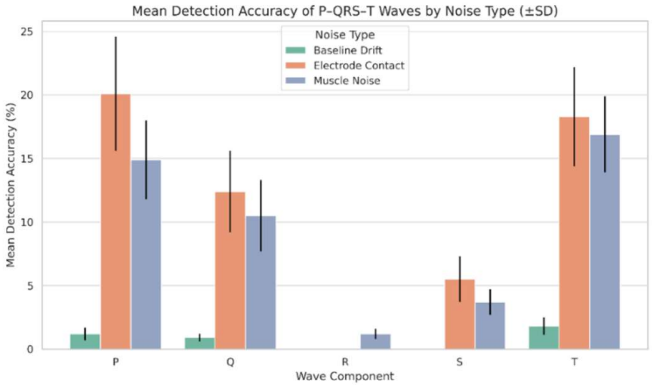

Fig. 3. Detection Accuracy of ECG Wave Components by Noise Type

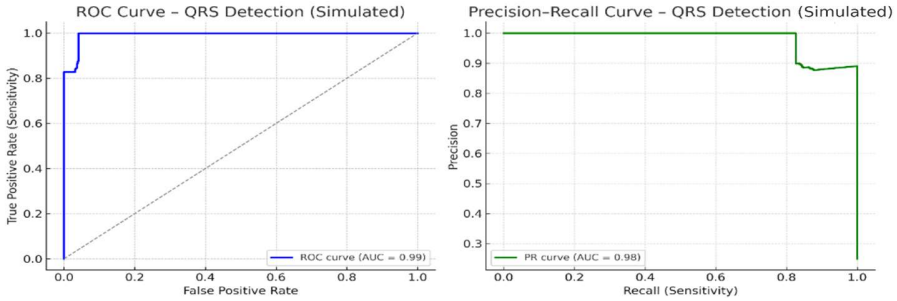

a) b)

Fig. 4. ROC and Precision–Recall Curves for QRS Complex Detection (Simulated used data form Table 1).

against varying noise types remains limited. To address these limitations, future research should explore hybrid approaches that integrate classical filtering techniques with deep learning models [4], [6], [29]. Such integration could enhance noise resilience and improve the reliable detection of ECG components – most critically, the QRS complex, which holds paramount clinical importance.

As depicted in the tables and figures, the method combines information from two filtered signal channels, following strategies similar to those in [7], [18], [30]. One channel is processed with a Chebyshev Type II filter optimized for QRS complex detection, while the other employs low-pass and high-pass filters to extract the P and T waves.

The dataset includes signals corrupted with baseline drift, electrode contact noise, and muscle noise at SNR levels of 5, 10, and 15 dB, with three signals per noise type and level. Each table entry corresponds to an individual signal, and the final column (ξ) indicates the average information loss (%) during data fusion. The arithmetic mean losses calculated across noise types are:

- 0.08 % for baseline drift,
- 10.07 % for electrode contact noise, and
- 5.32 % for muscle noise.

6. CONCLUSION

This study demonstrates the positive impact of filter fusion techniques on improving the automatic detection of P-QRS-T complexes in ECG signals recorded in maritime environments. The experimental results suggest that the combined use of low-pass, high-pass, and Chebyshev Type II filters contributes to improved accuracy in detecting key cardiac components – even under conditions specific to the maritime domain, such as motion-induced artifacts and electromagnetic interference.

Key observations indicate that integrating multiple filtering strategies enhances signal clarity and supports more robust and dependable cardiac monitoring for seafarers. This improved detection capability has important implications for timely diagnosis and medical intervention during cardiac events at sea, thereby supporting the health, safety, and operational readiness of maritime personnel.

Moreover, the study highlights the practical value of advanced ECG signal processing methods in the context of IoT-based health monitoring systems. When deployed in remote and dynamic environments – such as onboard vessels – these systems can offer improved real-time cardiac surveillance, enhancing medical autonomy and emergency response.

The differences in detection accuracy observed across various noise types suggest potential statistical relevance; however, formal significance testing was not conducted in this work.

In conclusion, the application of filter fusion methods in ECG signal analysis presents a meaningful step toward improving maritime telemedicine. While the study does not introduce a novel algorithm, it showcases a practical and effective approach to addressing common challenges in ECG monitoring at sea and contributes to the development of reliable onboard healthcare and emergency systems for seafarers.

The results of the proposed dual-channel merging method for detecting P-QRS-T complexes are encouraging. The average information loss remains low in signals affected by baseline drift (0.08 %) and skeletal muscle noise (5.32 %), with moderately higher values for electrode contact noise (10.07 %). These findings support the approach's potential, although further refinement is warranted.

While the study utilizes a synthetic ECG dataset with artificially added noise, future validation using real clinical data is necessary to assess its generalizability under operational maritime conditions.

To summarize the practical implications of the proposed method, the main technical advantages and limitations are outlined in the table 2.

Table 2. Pros and Cons of the Proposed Method

Advantages	Limitations
Lightweight and computationally efficient; suitable for embedded/IoT devices	Lower accuracy in QRS detection under certain noise types (e.g., contact noise)
Does not require large datasets or complex model training	Performance is below state-of-the-art AI in clinical-grade applications
Modular design; easy integration with existing IoT healthcare systems	Evaluated on synthetic data only; lacks real-world clinical validation

Overall, this work provides a solid foundation for the continued development of automated ECG analysis systems adapted to the specific healthcare needs of seafarers.

7. FUTURE WORK DIRECTIONS

Future research will aim to enhance the proposed ECG signal processing approach through several key directions. First, integrating adaptive filtering techniques with real-time learning algorithms is expected to improve the robustness of QRS complex detection under variable noise conditions. Validation on real maritime ECG datasets will be essential to assess the generalizability and clinical relevance of the method in operational settings.

In addition, the development of hardware prototypes for onboard deployment will support real-time implementation in maritime telemedicine systems. Efforts will also be directed toward minimizing detection errors, particularly for QRS complexes, and expanding the system's applicability to broader physiological monitoring tasks (e.g., respiratory or muscular activity).

A summarized roadmap for future development includes:

- Refining filter parameters and detection algorithms;
- Expanding the dataset for broader statistical analysis;
- Exploring integration with deep learning models and real-time onboard systems;
- Evaluating long-term performance in real-world maritime settings.
-

Source of funding: *This research paper has received funding from Ministry of Education and Science of the Republic of Bulgaria under the National Science Program "SECURITY AND DEFENSE", in implementation of the Decision of the Council of Ministers of the Republic of Bulgaria No: 731/21.10.2021 and according to Agreement No: D01-74/19.05.2022*

Author contributions: *research concept and design, V.E.A.; Collection and/or assembly of data, V.E.A.; Data analysis and interpretation, V.E.A.; Writing the article, I.Y.I.; Critical revision of the article, I.Y.I.; Final approval of the article, I.Y.I.*

Declaration of competing interest: *The authors declare that they have no known competing financial interests or personal relationships that could have appeared to influence the work reported in this paper.*

REFERENCES

1. Abdulhady AA, Nergz SM, Maryam K, Safar MA, Zrar KA, Halgurd SM. Electrocardiogram heartbeat classification using convolutional neural network-k Nearest Neighbor. ARO-The Scientific Journal Of Koya University. 2024;15(1):61-67. https://doi.org/10.14500/aro.11444.
2. Hatamian A, Farshidi F, Ghobadi C, Nourinia J, Mostafapour E. Improving the quality of ECG signal using wavelet transform and adaptive filters. J. Appl. Res. Electr. Eng., 2023;2(1):45-53. https://doi.org/0.22055/jaree.2022.37567.1030.
3. Atanasov V, Sivkov Y, Velikov N. An approach of feature extraction of ECG signal of CLAS database. Proc

Int Conf Biomed Innovations Appl (BIA). 2020:93–96. https://doi.org/10.1109/BIA50171.2020.9244497.
4. Belkadi MA, Daamouche A, Melgani F. A deep neural network approach to QRS detection using autoencoders. Expert Systems with Applications. 2021;184(115528). https://doi.org/10.1016/j.eswa.2021.115528.
5. Brik Y, Djerioui M, Attallah B. Efficient heart disease diagnosis based on twin support vector machine. Diagnostyka. 2021;22(3):3-11. https://doi.org/10.29354/diag/139241.
6. Ding C, Wang S, Jin X, Wang Z, Wang J. A novel transformer-based ECG dimensionality reduction stacked auto-encoders for arrhythmia beat detection. Medical Physics. 2023;52(6):5297-5932. https://doi.org/10.1002/mp.16534.
7. Ding Z, Vishu KC, Mohammad MK. ECG Signal Denoising Using Multi-scale Patch Embedding and Transformers. ICML 2024 Next Generation of Sequence Modeling Architectures Workshop. https://doi.org/10.48550/arXiv.2407.11065.
8. Duranta D, Rizwan A, Kiranyaz S, Gabbouj M. Enhancing atrial fibrillation detection accuracy: A wavelet transform filtered single lead ECG signal analysis with artificial neural networks and novel feature extraction. Mach Learn Appl. 2023;12:100472. https://doi.org/10.1016/j.mlwa.2023.100472.
9. Hulsenboom ADJ, Verdurmen KMJ, Vullings R, van der Hout-van der Jagt MB, Kwee A. Relative versus absolute rises in T/QRS ratio by ST analysis of fetal electrocardiograms in labour: A case-control pilot study. PloS ONE. 2019;14(3):e0214357. https://doi.org/10.1371/journal.pone.0214357.
10. Jan MA, Zhang W, Khan F, Abbas S, Khan R. Lightweight and smart data fusion approaches for wearable devices of the Internet of Medical Things. Information Fusion. 2023;103:102076. https://doi.org/10.1016/j.inffus.2023.102076.
11. Jenkal W, Latif R, Laaboubi M. ECG Signal denoising using an improved hybrid DWT-ADTF approach. Cardiovascular Engineering and Technology. 2024;15 (1):77-94. https://doi.org/10.1007/s13239-023-00698-8.
12. Iliev IY, Atanasov V. Electrocardiogram (ECG) signal processing. Mendeley Data. 2025;V1(2025). https://doi.org/10.17632/kxcfckmgb2.1.
13. Kim D, Lee KR, Lim DS, Lee KH, Lee SJ, Kim DY, Sohn CB. A novel hybrid CNN-transformer model for arrhythmia detection without R-peak identification using stockwell transform. Scientific Reports. 2025;15(1), 7817. https://doi.org/10.1038/s41598-025-92582-9.
14. Larsson TJ, Lindquist C. Traumatic fatalities among Swedish seafarers 1984-1988. Saf Sci. 1992;15(3):173–82. https://doi.org/10.1016/0925-7535(92)90003-I.
15. Lin M, Hong Y, Hong S, Zhang S. Discrete wavelet transform based ECG classification using gcForest: A deep ensemble method. Technology and Health Care. 2024;21:S95-S105. https://doi.org/10.3233/THC-248008.
16. Malik, SA, et al. An Iterative Filtering Based ECG Denoising Using Lifting Wavelet Transfor m Technique. ELECTRONICS. 2023; 12(2), 387. https://doi.org/10.3390/electronics12020387.
17. McSharry P, Clifford GD, Tarassenko L, Smith L. A dynamical model for generating synthetic electrocardiogram signals. IEEE Trans Biomed Eng. 2003;50(3):289–94. https://doi.org/10.1109/TBME.2003.808805.
18. Morteza M, Foad H. Identification of cardiovascular diseases through ECG classification using wavelet transformation. MBDI. 2024 (preprint/under review). https://doi.org/10.48550/arXiv.2404.09393.
19. Praveena HD, Sudha K, Geetha P, Venkatanaresh M. Comprehensive time-frequency analysis of noisy ECG signals – A review. Cardiometry. 2022. https://doi.org/10.18137/cardiometry.2022.24.271275.
20. Rizwan A, Priyanga P, Abualsauod EH, Zafrullah SN, Serbaya SH, Halifa A. A machine learning approach for the detection of QRS complexes in electrocardiogram (ECG) using discrete wavelet transform (DWT) algorithm. Comput Intell Neurosci. 2022;2022:9023478. https://doi.org/10.1155/2022/9023478.
21. Roberts SE, Jaremin B. Cardiovascular disease mortality in British merchant shipping and among British seafarers ashore in Britain. Int Marit Health. 2010;61(3):107–116.
22. Safdar M, Nowak R, Palka P. Pre-Processing techniques and artificial intelligence algorithms for electrocardiogram (ECG) signals analysis: A comprehensive review. Computers in Biology and Medicine. 2024;170:107908. https://doi.org/10.1016/j.compbiomed.2023.107908.
23. Soumiaa M, El HS, Mansouri M. The use of the multi-scale discrete wavelet transform and deep neural networks on ECGs for the diagnosis of 8 cardio-bascular diseases. Mendel Self Computing Journal. 2022;28(2): 62-66. https://doi.org/10.13164/mendel.2022.2.062.
24. Sun LC, Lee CC, Ke HY, Wei CY, Lin KF, Lin SS, Hsin H, Chen PN. Deep learning for the classification of atrial fibrillation using wavelet transform-based visual images. BMC Med Inform Decis Mak. 2025;22(349). https://doi.org/10.1186/s12911-025-02872-5.
25. Wang J, He F, Sun S. Construction of a new smooth support vector machine model and its application in heart disease diagnosis. Plos One. 2023;18(2) e0280804. https://doi.org/10.1371/journal.pone.0280804.
26. World Health Organization. Cardiovascular diseases (CVDs). World Health Organization; 2021. Available from (accessed at 05.05.2025): https://www.who.int/news-room/fact-sheets/detail/cardiovascular-diseases-(cvds).
27. Xiaohong Y, Yuanqi H, Qiang L. Automatic multichannel electrocardiogram record classification using XGBoost fusion model. front. Physiol. 2022;13: (840011). https://doi.org/10.3389/fphys.2022.840011.
28. Zhang Q, Chen Z, Liu G, Zhang W, Du Q, Tan J, Gao Q. Artificial intelligence clinicians can use chest computed tomography technology to automatically diagnose coronavirus disease 2019 (COVID-19) Pneumonia and Enhance Low-Quality Images. Infect Drug Resist, 2021-24(14):671-687. https://doi.org/10.2147/IDR.S296346.
29. Zhao W, Li Z, Hu J, Ma Y. A simple and effective deep neural network based QRS complex detection method on ECG signal. Frontiers in Physiology. 2024;15:1384356. https://doi.org/10.3389/fphys.2024.1384356.

30. Zhang J, Liang D, Liu A, Gao M, Chen X, Zhang X, Chen X. MLBF-Net: A multi-lead-branch fusion network for multi-class arrhythmia classification using 12-Lead ECG.MBDI. 2020. https://doi.org/10.48550/arXiv.2008.07263;
31. Zivaljevic D, Stamenkovic N, Stojanovic N. Optimum Chebyshev filter whit an equalised group delay response. International Journal of Electronics. 2023;110(10): 1834-1848. https://doi.org/10.1080/00207217.2022.2118854;
32. Zholmagambetova B, Mazakov T, Jomartova S, Izat A, Bibalayev O. Methods of extracting electrocardiograms from electronic signals and images in the Python environment. Diagnostyka. 2020;21(3):95-101. https://doi.org/10.29354/diag/126398.

Veselin Evgeniev ATANASOV received his Ph.D. degree in Automated Information Processing and Control Systems from the Nikola Vaptsarov Naval Academy, Varna, Bulgaria. He is currently an Assistant Professor at the Department of Electronics, Faculty of Engineering, Nikola Vaptsarov Naval Academy. His main research interests are in biomedical signal processing, sensor networks, IoT communication, and maritime applications of information and communication technologies.
E-mail: veselin.atanasov@naval-acad.bg

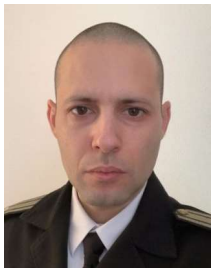

Iliyan Yordanov ILIEV received his Ph.D. degree in Communication Engineering and Technologies from the Technical University of Varna, Bulgaria. He is currently an Assistant Professor at the Department of Information Technologies, Faculty of Engineering, Nikola Vaptsarov Naval Academy. His main research interests are in computer science, communication and radar systems, and cryptographic security .
E-mail: i.y.iliev@naval-acad.bg

Appendix A

Table A 1. Result for Baseline drift.

	Result of automatic detections after Chebyshev filter						Result of automatic detections after Low, High filters					
	SNR_{in}	**DP**	**DQ**	**DR**	**DS**	**DT**	**SNR_{in}**	**DP**	**DQ**	**DR**	**DS**	**DT**
Signal 1	5,02	5,56	**1,85**	**0,00**	**0,00**	16,67	5,02	**0,00**	1,85	0,00	0,00	**1,85**
Signal 2	4,94	2,70	**0,00**	**0,00**	**0,00**	9,46	4,94	**0,00**	14,86	0,00	0,00	**0,00**
Signal 3	5,07	1,27	**0,00**	**0,00**	**0,00**	5,06	5,07	**0,00**	36,71	0,00	6,33	**0,00**
Signal 1	10,37	0,00	**0,00**	**0,00**	**0,00**	5,56	10,37	**0,00**	0,00	0,00	0,00	**0,00**
Signal 2	10,22	0,00	**0,00**	**0,00**	**0,00**	0,00	10,22	**0,00**	36,71	0,00	2,53	**0,00**
Signal 3	10,05	0,00	**0,00**	**0,00**	**0,00**	5,41	10,05	**0,00**	14,86	0,00	0,00	**0,00**
Signal 1	15,39	0,00	**0,00**	**0,00**	**0,00**	0,00	15,39	**0,00**	0,00	0,00	0,00	**0,00**
Signal 2	15,31	0,00	**0,00**	**0,00**	**0,00**	0,00	15,31	**0,00**	37,97	0,00	2,53	**0,00**
Signal 3	15,23	0,00	**0,00**	**0,00**	**0,00**	1,35	15,23	**0,00**	16,22	0,00	0,00	**0,00**

Table A 2. The average information loss for Baseline drift.

	SNR_{in}	**ξ**
Signal 1	5,02	0,74074
Signal 2	4,94	0,00000
Signal 3	5,07	0,00000
Signal 1	10,37	0,00000
Signal 2	10,22	0,00000
Signal 3	10,05	0,00000
Signal 1	15,39	0,00000
Signal 2	15,31	0,00000
Signal 3	15,23	0,00000
		0,08230

Table A 3. Result for Poor electrode contact.

	Result of automatic detections after Chebyshev filter						Result of automatic detections after Low, High filters					
	SNR_{in}	**DP**	**DQ**	**DR**	**DS**	**DT**	**SNR_{in}**	**DP**	**DQ**	**DR**	**DS**	**DT**
Signal 1	5,22	57,41	**3,70**	**0,00**	**0,00**	59,26	5,22	**61,11**	7,41	0,00	3,70	**57,41**
Signal 2	5,00	55,70	**1,27**	**0,00**	**1,27**	44,30	5,00	**50,63**	43,04	0,00	25,32	**43,04**
Signal 3	5,10	52,70	**1,35**	**0,00**	**1,35**	52,70	5,10	**50,00**	29,73	0,00	9,46	**56,76**
Signal 1	10,28	20,37	**1,85**	**0,00**	**0,00**	25,93	10,28	**18,52**	1,85	0,00	0,00	**24,07**
Signal 2	10,14	17,72	**0,00**	**0,00**	**0,00**	13,92	10,14	**13,92**	39,24	0,00	12,66	**16,46**
Signal 3	10,49	16,22	**0,00**	**0,00**	**0,00**	27,03	10,49	**17,57**	21,62	0,00	4,05	**25,68**
Signal 1	15,17	7,41	**0,00**	**0,00**	**0,00**	18,52	15,17	**5,56**	0,00	0,00	0,00	**11,11**
Signal 2	15,47	6,33	**0,00**	**0,00**	**0,00**	5,06	15,47	**6,33**	0,00	0,00	0,00	**5,06**
Signal 3	15,33	2,70	**0,00**	**0,00**	**0,00**	13,51	15,33	**2,70**	17,57	0,00	2,70	**6,76**

Table A 4. The average information loss for Poor electrode contact.

	SNR_{in}	**ξ**
Signal 1	5,22	24,44444
Signal 2	5,00	19,24051
Signal 3	5,10	21,89189
Signal 1	10,28	8,88889
Signal 2	10,14	6,07595
Signal 3	10,49	8,64865
Signal 1	15,17	3,33333
Signal 2	15,47	2,27848
Signal 3	15,33	1,89189
		10,74378

Table A 5. Result for Muscle noise.

	Result of automatic detections after Chebyshev filter						Result of automatic detections after Low, High filters					
	SNR_{in}	**DP**	**DQ**	**DR**	**DS**	**DT**	**SNR_{in}**	**DP**	**DQ**	**DR**	**DS**	**DT**
Signal 1	4,93	44,44	**9,26**	**12,96**	**7,41**	45,35	4,93	**11,11**	5,56	0,00	1,85	**16,67**
Signal 2	4,92	0,12	**37,97**	**7,59**	**2,53**	1,27	4,92	**11,39**	45,57	1,27	8,86	**17,72**
Signal 3	5,09	0,13	**28,38**	**0,00**	**1,35**	4,05	5,09	**5,41**	25,68	0,00	8,11	**17,57**
Signal 1	10,14	24,07	**1,85**	**1,85**	**1,85**	31,48	10,14	**3,70**	0,00	0,00	0,00	**7,41**
Signal 2	10,09	18,99	**3,80**	**0,00**	**1,27**	26,58	10,09	**6,33**	43,04	0,00	2,53	**10,13**
Signal 3	10,06	12,16	**0,00**	**0,00**	**0,00**	22,97	10,06	**1,35**	18,92	0,00	2,70	**5,41**
Signal 1	15,18	18,52	**0,00**	**0,00**	**0,00**	16,67	15,18	**1,85**	0,00	0,00	0,00	**1,85**
Signal 2	15,18	7,59	**1,27**	**0,00**	**0,00**	18,99	15,18	**1,27**	43,04	0,00	1,27	**1,27**
Signal 3	15,31	4,05	**0,00**	**0,00**	**0,00**	12,16	15,31	**0,00**	18,92	0,00	0,00	**0,00**

Table A 6. The average information loss for Muscle noise.

	SNR_{in}	**ξ**
Signal 1	4,93	11,48148
Signal 2	4,92	15,44304
Signal 3	5,09	10,54054
Signal 1	10,14	3,33333
Signal 2	10,09	4,30380
Signal 3	10,06	1,35135
Signal 1	15,18	0,74074
Signal 2	15,18	0,75949
Signal 3	15,31	0,00000
		5,32820